Epidemiol. Infect. (2012), **140**, 1557–1568. © Cambridge University Press 2011
doi:10.1017/S0950268811002226

Using experimental human influenza infections to validate a viral dynamic model and the implications for prediction

S. C. CHEN[1,2], S. H. YOU[3], C. Y. LIU[1], C. P. CHIO[3] AND C. M. LIAO[3]*

[1] *Department of Public Health, Chung Shan Medical University, Taichung, Taiwan, ROC*
[2] *Department of Family and Community Medicine, Chung Shan Medical University Hospital, Taichung, Taiwan, ROC*
[3] *Department of Bioenvironmental Systems Engineering, National Taiwan University, Taipei, Taiwan, ROC*

(*Accepted 12 October 2011; first published online 14 November 2011*)

SUMMARY

The aim of this work was to use experimental infection data of human influenza to assess a simple viral dynamics model in epithelial cells and better understand the underlying complex factors governing the infection process. The developed study model expands on previous reports of a target cell-limited model with delayed virus production. Data from 10 published experimental infection studies of human influenza was used to validate the model. Our results elucidate, mechanistically, the associations between epithelial cells, human immune responses, and viral titres and were supported by the experimental infection data. We report that the maximum total number of free virions following infection is 10^3-fold higher than the initial introduced titre. Our results indicated that the infection rates of unprotected epithelial cells probably play an important role in affecting viral dynamics. By simulating an advanced model of viral dynamics and applying it to experimental infection data of human influenza, we obtained important estimates of the infection rate. This work provides epidemiologically meaningful results, meriting further efforts to understand the causes and consequences of influenza A infection.

Key words: Immune system, infection, influenza virus, modelling, viral dynamics.

INTRODUCTION

A variety of mathematical and computational models have been proposed for elucidating the nonlinear transmission dynamics of epidemics and for enhancing our understanding of the spread of diseases and the immune responses that subsequently occur within the infected host [1–3]. To date, important results have been obtained from mathematical modelling of viral dynamics for human immunodeficiency [4–6], hepatitis B [7, 8], hepatitis C [9] and influenza viral infections [10–12].

The kinetics of the human influenza virus life-cycle is a complex process that involves many important factors, including the rate at which epithelial cells are produced and infected, and the rate at which viruses are produced from such epithelium. These said processes are influenced by intrinsic cellular dynamics and extrinsic immunological factors. Thus, computer simulation would be a valuable tool to assess the potential contribution and relative importance of each factor, especially when unexpected scenarios are difficult to replicate experimentally [10, 12].

* Author for correspondence: Dr Chung-Min Liao, Department of Bioenvironmental Systems Engineering, National Taiwan University, Taipei, Taiwan 10617, ROC.
(Email: cmliao@ntu.edu.tw)

Table 1. *Summary of used experimental human influenza A(H1N1) infection data*

Age group (yr)	Size of study subgroups (*N*)	Virus	Inocul. dose ($TCID_{50}$)	Infected *N* (% of subgroup size)	Shedding virus *N* (% of infected)	Mean virus shedding duration (day)	Reference
18–25	9	A/California/10/78/H1N1	$10^{4·5}$	8 (89)	8 (100)	n.a.	[33]
18–45	16	A/Kawasaki/86/H1N1	10^{7}	16 (100)	16 (100)	2·8	[34]
18–33	59	A/Texas/36/91/H1N1	10^{5}	49 (83)	49 (100)	2	[16]
19–40	19	A/Texas/36/91/H1N1	10^{5}	19 (100)	19 (100)	n.a.	[14]
18–40	14	A/Texas/36/91/H1N1	10^{6}	14 (100)	14 (100)	n.a.	[35]
19–33	8	A/Texas/36/91/H1N1	10^{5}	8 (100)	8 (100)	4·6	[17]
19–35	8	A/Texas/36/91/H1N1	10^{5}	8 (100)	8 (100)	n.a.	[18]
18–40	13	A/Texas/36/91/H1N1	10^{6}	13 (100)	n.a.	4·5	[15]
19–40	14	A/Texas/36/91/H1N1	10^{5}	14 (100)	14 (100)	5·1	[29]
18–45	18	A/Texas/36/91/H1N1	10^{6}	17 (94)	17 (100)	3·2	[22]

$TCID_{50}$, Median tissue culture infective dose; *N*, sample size; n.a., not available.

Modelling the dynamics of influenza virus infection has progressed significantly. Baccam *et al.* [10] provided two models describing the kinetics of such infection in humans: a target cell-limited model and a target cell-limited model with delayed virus production. These authors used data from experimentally infected volunteers to estimate various parameters of the viral life-cycle using mathematical models. Their findings suggested that modelling with the target cell-limited model with delayed virus production was more realistic because infected cells began producing influenza virus for nearly 5 h. In addition, Chang & Young [12] developed a model based on simple scaling laws as delineated by ordinary differential equations that describes the time-courses of the numbers of infectious viral particles, activated cytotoxic T-lymphocytes (CTLs), interferon (IFN) molecules, infected cells, uninfected cells, and the subset of uninfected cells that are protected from viral infection by IFN. They found that the rise time, duration, and the severity of influenza A infection could be expressed as a function of the initial viral load with relevant parameters based on the developed scaling laws.

A target cell-limited model with delayed virus production can also be incorporated with an indoor aerosol transmission model and a population dynamic susceptible-exposed-infective-recovery model to quantify the influenza infection risk in the human upper respiratory tract [13]. Chen *et al.* [13] revealed that the influenza infection risk in a school setting could be estimated appropriately by combining the viral kinetics and different exposure parameters with environmental factors.

Experimental viral infection of human influenza A can be utilized to investigate local and systemic cytokine responses during the infection period [14], even after oral or intravenous neuraminidase inhibitor administration [15–18]. Different experimental trials have assessed dosing, formulation, and host responses on daily viral titre, viral shedding, peak titre, days of shedding, and clinical symptom scores. However, consideration of the variations in the selected coefficient from influenza infection data remains a major analytical challenge for validating viral dynamics models.

In the present work, for the practical aim of estimating system parameters from experimental infection data of human influenza, we sought to develop a mathematical model by combining the target cell-limited model with delayed virus production [10] with a model that considers the effects of the immune response, including IFN and CTL factors [12]. More importantly, this modified model was used to perform sensitive analysis and was validated with experimental infection data of human influenza A. We believe that such a framework could be incorporated explicitly into influenza control modelling schemes.

MATERIALS AND METHODS

Study data

Ten published experimental infection studies of human influenza A(H1N1) were used as the study data (see Table 1). Briefly, participants were inoculated intranasally (0·25 ml per nostril) with H1N1 on day 0 with a dose ranging from $10^{4·5}$ to 10^{7} of tissue culture

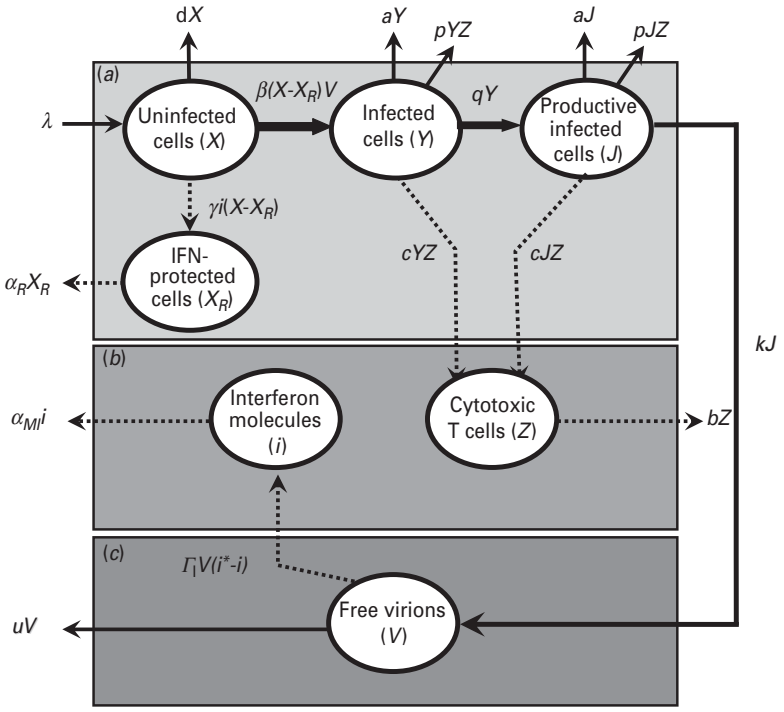

Fig. 1. Schematic representation showing the pathway interactions of influenza virus infecting human lung epithelial cells at: (*a*) the epithelial cell level; (*b*) the human immune response level; and (*c*) the virus level. The definition of symbols and their detailed descriptions are given in the text and Table 2.

infective dose ($TCID_{50}$). The test age groups were healthy young men and women. The number of infected people ranged from eight to 59 with shedding durations ranging from 2 to 5·1 days. Nasal washings were collected before viral inoculation for the detection of virus infection and collected from days 0 to 8 for virus isolation.

The age groups, size of study subgroups, numbers of infected people, numbers of shed virus and shedding durations were all recorded. The main differences were found in inoculated dose, experimental sample size, and the mean virus shedding duration. For safety considerations, young and healthy men and women were used. Sex distinctions were deemed irrelevant. A high percentage of the subgroup became infected, and, of those infected, nearly 100% shed virus. Eight published studies used the same virus strain.

We estimated the daily-based average viral titres (log $TCID_{50}$ ml^{-1}) from the published study data from day 0 (time of inoculation) to day 8. Statistical analysis was performed using free virions from our modified viral dynamics model and daily-based average viral titres from the experimental influenza infections. Didger 4 software (Golden Software Inc., USA) was used for data collection from the published studies.

Model

Viral dynamics models have several assumptions [1]: (1) uninfected cells encounter free virus, becoming infected cells; (2) the rate of production of new infected cells is proportional to the product of the density of uninfected cells multiplied by the density of free virions; (3) free virions are produced by infected cells; (4) uninfected cells, infected cells and free virions die at certain rates; and, (5) uninfected cells are constantly replaced by the system.

By studying a model of influenza viral dynamics that builds on past well-developed models [10, 12], we explored the consequences of host–pathogen interactions at three levels: (*a*) the epithelial cell level; (*b*) the human immune response level (including the role of IFN and CTLs); and, (*c*) the virus level. The essential features of this model are depicted in Figure 1.

Briefly, after influenza A virus infects epithelial cells, progeny virions are usually not detected for 6–8 h [10]. This delay in the production of free virions can be modelled by defining two separate populations

of infected epithelial cells: one population (Y) is infected but not yet producing virus and the second population (J) is actively producing virus, a so-called productive infection [10]. Therefore, at the epithelial cell level (Fig. 1*a*), uninfected cells (X) can be infected by free virions (V), becoming a cell population as defined by Y. After 6–8 h, following viral entry and replication, this epithelial population becomes capable of actively producing virions as defined by J.

The rate λ (d^{-1}) is the equilibrium between the production rate of epithelial cells and their natural death at rate $-dX$. The conversion of uninfected to infected cells is defined by the rate $-\beta(X-X_R)V$, where β (d^{-1} virion^{-1}) represents the infection rate of an unprotected epithelial cell per virion and X_R represents IFN-protected cells. The rate of change of population Y contains the same infection rate term, $\beta(X-X_R)V$, and a decay term, $-aY$, due to viral cytolytic effects with a (d^{-1}) representing the reciprocal of the infected epithelial cell's lifespan. An additional loss term, $-pYZ$, describes the action of CTLs with p (d^{-1} CTL^{-1}) representing the rate of CTL-induced destruction of infected epithelial cells. The transition rate q (d^{-1}) represents the transition from Y to J. Here, we assumed that a decay term $-aJ$ represents viral cytolytic effects, and an additional loss term $-pJZ$ represents the action of CTLs on the system. The transition rate k (d^{-1} infected cell^{-1}) represents infected epithelial cells (J) that become capable of producing free virions (V). At the human immune response level (Fig. 1*b*), CTLs (Z) can be induced and activated by Y and J. The rate of change of virus-specific CTLs contains a production rate, $c(Y+J)Z$, and a natural decay rate, $-bZ$, where c (d^{-1} infected cell^{-1}) is the production rate of induced CTLs per infected epithelial cell, and b (d^{-1}) is the reciprocal of the CTL lifespan. Uninfected epithelial cells (X) that become IFN-protected (X_R) are described by the production term $\gamma i(X-X_R)$, where γ (d^{-1} IFN^{-1}) represents the rate constant for the induction of the IFN-induced anti-viral state. In addition, the term, $-\alpha_R X_R$, with α_R (d^{-1}) representing the rate of IFN-protected epithelial cell decay, represents the natural decay term.

IFN cytokines, represented by the total number of IFN molecules, i, can protect cells (X_R) from becoming infected. The rate of change in the number of IFN molecules contains both a natural decay term, $-\alpha_{MI} i$, and a production term, $\Gamma_I V(i^*-i)$, which describes the virus-induced activation of IFN-producing macrophages. The term α_{MI} (d^{-1}) is the rate of loss of IFN-producing macrophages. The term Γ_I (d^{-1} virion^{-1}) is the induction rate for IFN production. The term i^* is the effective production rate number for IFN.

The present model used free virions in epithelial cells (V) to represent the virus level (Fig. 1*c*). The term kJ describes the production of virions from infected cells at rate k, and the term $-uV$ describes the natural decay of the virion at a rate u.

The system of ordinary differential equations corresponding to the model in Figure 1 and based on previous work are as follows [10, 12]:

$$\frac{dX}{dt} = \lambda - dX - \beta(X-X_R)V, \tag{1}$$

$$\frac{dY}{dt} = \beta(X-X_R)V - aY - qY - pYZ, \tag{2}$$

$$\frac{dJ}{dt} = qY - aJ - pJZ, \tag{3}$$

$$\frac{dV}{dt} = kJ - uV, \tag{4}$$

$$\frac{dZ}{dt} = c(Y+J)Z - bZ, \tag{5}$$

$$\frac{dX_R}{dt} = \gamma i(X-X_R) - \alpha_R X_R, \tag{6}$$

$$\frac{di}{dt} = \Gamma_I V(i^*-i) - \alpha_{MI} i. \tag{7}$$

Model implementation

The definitions, symbols, input values, and expected physiological ranges of parameters in this influenza model are summarized in Table 2. The input parameters of biological characteristics were derived from experimentally infected volunteers [19–21]. The physiological ranges for individual differences could also be estimated.

To identify the most significant sensitive parameters in our model, we performed a sensitivity analysis for four parameters involving production rates λ and k with infection rate β and transition rate q, respectively. This quantitative analysis can show robustness of the effects of free virion dynamics when model assumptions are made and when key parameters are varied. The sensitivity analysis was performed by varying the key production and

Table 2. *Definition, symbols, input values, and expected physiological ranges of parameters in the modified influenza virus dynamic model*

Symbols	Definition and unit	Input value†	Range value‡
X_0	Equilibrium number of normal epithelial cells in upper six branches	10^9	—
λ	Equilibrium production rate of epithelial cells (d^{-1})	$6{\cdot}25 \times 10^7$	—
d	Reciprocal of epithelial cell lifespan (d^{-1})	0·0625	—
β	Infection rate of an unprotected epithelial cell per virion (d^{-1} virion^{-1})	10^{-10}	$3 \times 10^{-14} - 6 \times 10^{-10}$
a	Reciprocal of infected epithelial cell lifespan (d^{-1})	1	0·5–2
q	Transition rate from infected cells to productive infected cells (d^{-1})	4§	2–6§
p	Infected epithelial cell CTL-induced destruction rate (d^{-1} CTL^{-1})	10^{-10}	$4 \times 10^{-12} - 5 \times 10^{-10}$
V_0	Initial virus particles (virions)	10^7	—
k	Production rate of viruses by an infected epithelial cell (d^{-1} infected cell^{-1})	340	67–6700
u	Reciprocal of influenza A virus lifespan (d^{-1})	2	2–4
Z_0	Initial number of influenza A-specific CTLs in upper six branches	7×10^6	$0{\cdot}72 \times 10^6 - 7{\cdot}2 \times 10^6$
c	CTL-induced production rate of CTL per infected epithelial cell (d^{-1} infected cell^{-1})	$3{\cdot}6 \times 10^{-8}$‡	—
b	Reciprocal of CTL lifespan (d^{-1})	0·5	—
γ	Rate constant for induction of anti-viral state by IFN (d^{-1} IFN^{-1})	10^{-9}	$10^{-8} - 10^{-10}$
α_R	Rate of virus resistant epithelial cell decay (d^{-1})	1	—
Γ_I	Induction rate for IFN production (d^{-1} virion^{-1})	8×10^{-10}	—
i^*	Effective IFN production rate number	10^{10}	$7{\cdot}7 \times 10^7 - 7{\cdot}7 \times 10^{10}$
α_{MI}	Rate of loss of IFN-producing macrophages (d^{-1})	0·5	0·3–0·5

CTL, Cytotoxic T-lymphocyte; IFN, interferon.
† Adopted from Murphy *et al.* [19] (cited in Chang & Young [12]).
‡ All of the estimated physiological ranges shown are based on the parameter estimates in Bocharov & Romanyukha [20], except for the value of c which was directly obtained from Beauchemin *et al.* [21].
§ Adopted from Baccam *et al.* [10].

destruction rates of λ, q, k, and β, ranging from 0 to $6{\cdot}57 \times 10^7$ d^{-1}, 2–6 d^{-1}, 67–6700 d^{-1} infected cell^{-1}, and 3×10^{-14} to 6×10^{-10} d^{-1} virion^{-1}, respectively. Model validation was also performed based on the selected study data. Here we used a coefficient of determination (r^2) and P values as the quantitative criterion for the model validation. Model simulations were performed using Berkeley Madonna 8.0.1 (as developed by Robert Macey and George Oster of the University of California at Berkeley).

RESULTS

Influenza viral dynamics

We found that uninfected cells (X) decreased in number from the initial values of 10^9 cells by virtue of free virion infection whereas IFN-protected cells (X_R) increased rapidly at days 2–3 and reached a peak value of $8{\cdot}2 \times 10^8$ cells at day 3·4, showing an 89% protection by IFN at this time-point (Fig. 2*a*). On the other hand, the peak values of non-productive infected cells (Y) and productive infected cells (J) occurred at days 2·5 and 7 with $9{\cdot}55 \times 10^6$ cells and $3{\cdot}54 \times 10^7$ cells, respectively (Fig. 2*a*).

At the immune response level, the first responder to influenza A infection was IFN(i), with production of this cytokine beginning <2 h after viral infection, reaching a peak between days 3 and 4 (Fig. 2*b*). By contrast, CTL responders (Z) were much slower, showing peak activity at day 10 (Fig. 2*b*). At the virus level, a high viral titre appeared at day 2 and reached a peak value of $5{\cdot}96 \times 10^9$ virions by day 7 (Fig. 2*c*).

Human experimental viral titre concentration

Table 3 gives the daily-based average viral titres in the previous studies included in this report. Most viral titres were recorded on days 0–8, except the study by Barroso *et al.* [22] which sampled twice (in morning and afternoon) on days 1–3, and only once on days 4–7. In order to estimate the daily-based average viral titres, we used approximate values from this study [22]. The overall patterns started after day 1 and approached towards peak viral titres during

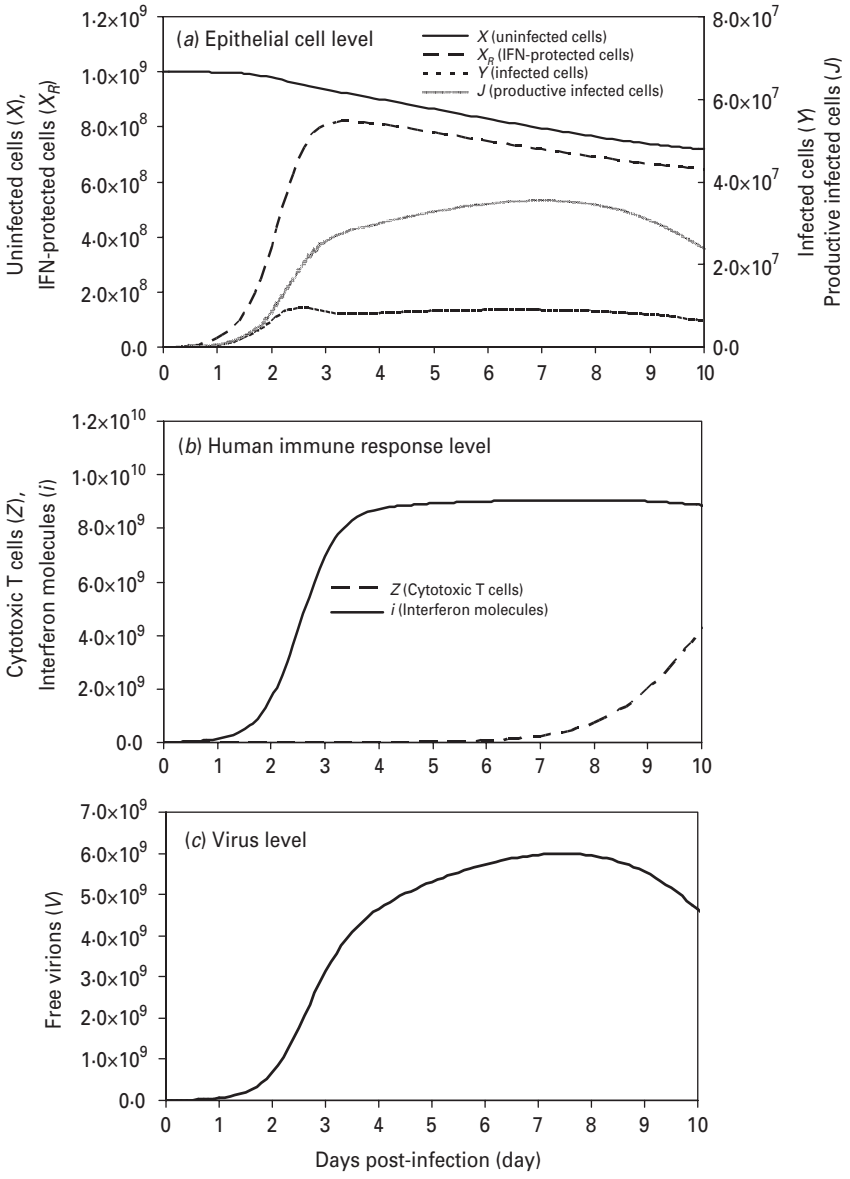

Fig. 2. Model influenza A variables at the three levels: (*a*) at the epithelial cell level: parameters include X (uninfected cells), X_R (IFN-protected cells), Y (infected cells), and J (productive infected cells); (*b*) at the human response level: parameters include Z (CTLs) and I (IFN molecules); (*c*) at the virus level: parameters include V (free virions) with an initial viral load of 10^7 virions. Input values of these parameters are presented in Table 2.

day 2 with a measure of $10^{3{\cdot}51}$ $TCID_{50}$ ml^{-1} and then slowly decreased to $<10^1$ $TCID_{50}$ ml^{-1} by day 6.

Parameter sensitivity analysis

To evaluate the variability of parameters that significantly contribute to free virions, sensitivity analyses were performed. The time-course of free virions was used to show the model's sensitivity to variations in parameters λ, q, k, and β, respectively (Fig. 3). When the modified influenza viral dynamics model was subjected to an input parameter of λ ranging from 0 to $6{\cdot}27\times10^7$ d^{-1}, free virions decreased accordingly after day 3 post-infection, whereas a similar effect on q was noted when parameters ranged from 2 to 6 d^{-1} (Fig. 3*a*, *b*).

We also found that the infection rates of uninfected cells (to become infected cells) increased when input parameters of the infection rate β were increased from 6×10^{-10} to 3×10^{-14} d^{-1} $virion^{-1}$. Similarly, free virions in epithelial cells increased with an increasing

Table 3. *Daily-based average viral titers (log $TCID_{50}$ ml^{-1}) which was estimated by the results of viral titres in experimental influenza virus infection*

Days post-infection									
0	1	2	3	4	5	6	7	8	Reference
0·013	0·019	1·86	1·66	1·17	0·74	0·78	0	0	[33]†
0·5	2·69	2·49	1·26	0·83	0·77	0·49	0	0	[34]†
0	0·97	2·71	2·71	1·90	0·82	0·54	0·40	0·17	[16]†
0·0058	1·86	3·77	3·34	2·60	2·50	1·32	0·81	0·16	[14]†
0	2	3·8	3·2	2·7	2·6	1·4	0·6	0·3	[35]†
0	1·99	3·41	2·65	2·17	0·76	0·25	0·44	0	[17]†
0·005	2·39	4	2·13	1·89	0·74	0	0	0	[18]‡
0	2·24	3·34	3·02	1·64	0·40	0	0	0	[15]‡
−0·5	1·87	3·62	3·12	2·69	2·53	1·22	0·16	−0·12	[29]†
0	2·14	2·68	2·45	1·51	0·82	0·14	0·05	0	[22]†
0·08	2·14	3·51	2·88	2·25	2·04	0·94	0·48	0·15	Average§
−0·08	2·15	3·52	2·87	2·30	2·22	0·97	0·29	−0·29	S.E.

† Mean values.
‡ Median values.
§ Arithmetic average of 10 viral titers (log $TCID_{50}$ ml^{-1}) on a specific day.

value of k, the virus production rate from infected epithelium (Fig. 3*c–f*).

Pearson correlation analysis [23] was used to determine the optimal parameter inputs, with the best statistical significance, between the daily-based average viral titres and the prediction of free virions that varied with physiological ranges of parameter input. Our results indicated that input values of $k=4000$ and $\beta=5\times10^{-10}$ resulted in a significant correlation between experimental human infection data shown in Table 3 and model predictions ($r=0{\cdot}99$, $P<0{\cdot}0001$) (Table 4, Fig. 4). This sensitivity analysis suggested that the infection rate of an unprotected epithelial cell (β) is likely to play an important role in shaping the viral dynamics, whereas the viral production rate from infected epithelial cells (k) is the second most sensitive parameter in this model.

Model validation

To test this prediction, we performed the model's validation with derived optimal estimates of production rate k and infection rate β values. Figure 4*a* shows the time-course of predicted free virions in epithelial cells with the optimal parameters of $k=4000$ and $\beta=5\times10^{-10}$ against the experimental data of daily-based average viral titres shown in Table 3. Generally, the results were in agreement with the experimental data trend, except on days 6–8 where a decreasing trend was noted. This may be due in part to individual immune variations in response to influenza virus. Moreover, with regard to Table 3, there were 2–6 missing data points of the daily-based average viral titres at days 6–8 post-infection.

This study also compared the predictive capacities for free virions among the target-cell limited model with delayed virus production [10], the immune response model [12] and our modified viral dynamics model (Fig. 4*b*). Our results indicated that our model fit experimental data of the dynamics of free virion production ($r^2=0{\cdot}99$, $P<0{\cdot}0001$) better than the target-cell limited model with delayed virus production ($r^2=0{\cdot}85$, $P=0{\cdot}0004$) and the immune response model ($r^2<0{\cdot}1$, $P=0{\cdot}955$) (Fig. 4*b*). This indicates our model as performing better than the others during validation. On the other hand, this study presents the results of viral dynamics modelling by considering the optimal input at $\beta=5\times10^{-10}$ (Table 4, Fig. 5*a*). Figure 5*b* shows the rapid rise in IFN at 1–2 days after introduction of the virus followed by a broad maximum between days 2 and 3. The IFN production begins within hours and peaks at between 72 and 92 h. Figure 5*c* shows the rapid rise in CTL immunity between days 3 and 6. Figure 5*d* shows that the maximum total number of free virions during infection is 10^3-fold higher than the initial number introduced ($V_0=10^7$).

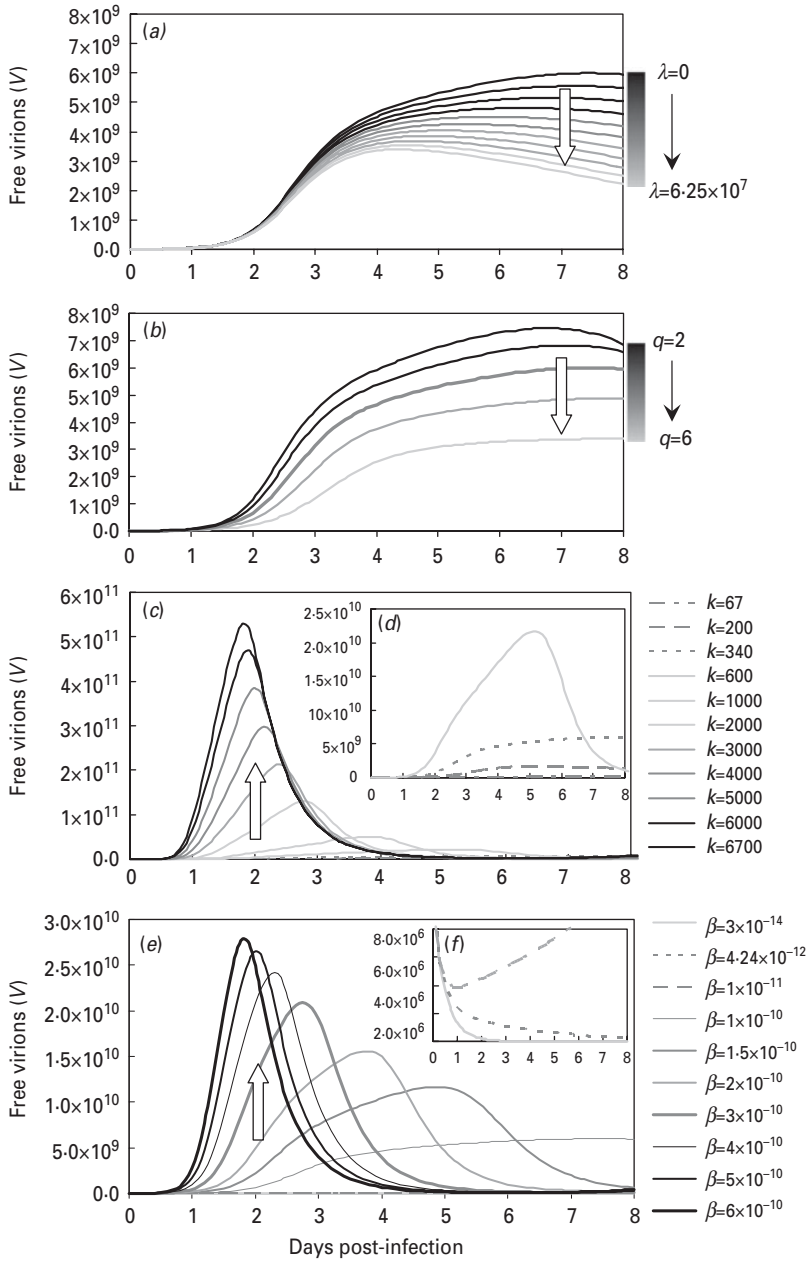

Fig. 3. Sensitivity analysis of λ [equilibrium production rate of epithelial cells (d^{-1})], q [transition rate from Y to J (d^{-1})], k [production rate of viruses from infected epithelial cells (d^{-1} infected cell^{-1})] and β [reciprocal of epithelial cell lifespan (d^{-1} virion^{-1})] are presented. The expected physiological ranges of these four parameters are given in Table 2.

DISCUSSION

Mathematical models have long been recognized as useful tools for exploring complicated relationships that underlie infectious disease transmission [24]. The accuracy of the predictions obtained from mathematical modelling depends on the accuracy of the estimated parameters used in the model. To this end, good parameter estimates are needed to understand and model the potential spread of influenza while the interpretation of data from experimental infection studies provides validation of mathematical model predictions for different influenza infection scenarios. Moreover, the dynamics of viral shedding and symptoms following influenza virus infection are key factors when considering epidemic control measures [10, 14].

Our study developed a modified viral dynamics model that builds on past models of a target cell-limited model with delayed virus production introduced by

Table 4. *Optimal Pearson correlation analysis between experimental human infection data* (*Table 3*) *and modelling results from the modified virus dynamic model*

Parameter	Input value (original value)	Optimal r	P value
Equilibrium production rate of epithelial cells, λ (d^{-1})	$6{\cdot}25 \times 10^{7}$ ($6{\cdot}25 \times 10^{7}$)	−0·43	0·2459
Transition rate from infected cells to productive infected cells, q (d^{-1})	2 (4)	−0·46	0·2077
Production rate of viruses by an infected epithelial cell, k (d^{-1} infected cell^{-1})	4000 (340)	0·996	<0·0001
Infection rate of an unprotected epithelial cell per virion, β (d^{-1} virion^{-1})	5×10^{-10} (10^{-10})	0·999	<0·0001

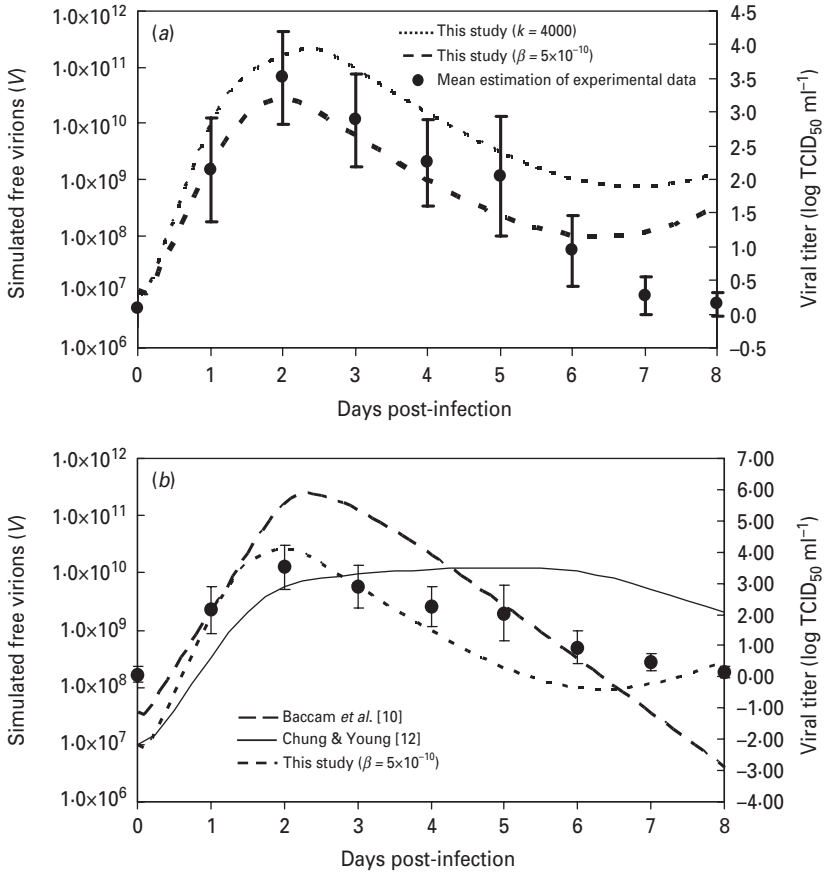

Fig. 4. (*a*) Model validation of the present virus dynamics model against the daily-based average viral titres data. (*b*) A comparison of our modified model with the target-cell limited model with delayed virus production [10] and the immune response model [12]. The data (mean ± S.E.) have the same values with a different scale as shown in Table 3.

Baccam *et al*. [10] and Chung & Young [12]. Here, we adopted these two models and compared the results by fitting the models to experimental human infection data. Results showed that our present model seemed to fit data better than each individual past model. Our results indicate a mechanistic explanation for the associations between epithelial cells, human immune responses, and virus dynamics. These mechanistic insights were supported by the experimental human infection results. Our study also revealed that the maximum total number of free virions ($V(t)$) during infection is 10^3-fold higher than that of the initial number introduced (V_0). This result is supported by previous research, indicating that this is within the range of 10–10^5 that has been observed in other experimental data [10, 17, 19, 20, 25–27]. Our model thus had higher performance when accounting for the human immune response level, which incorporated

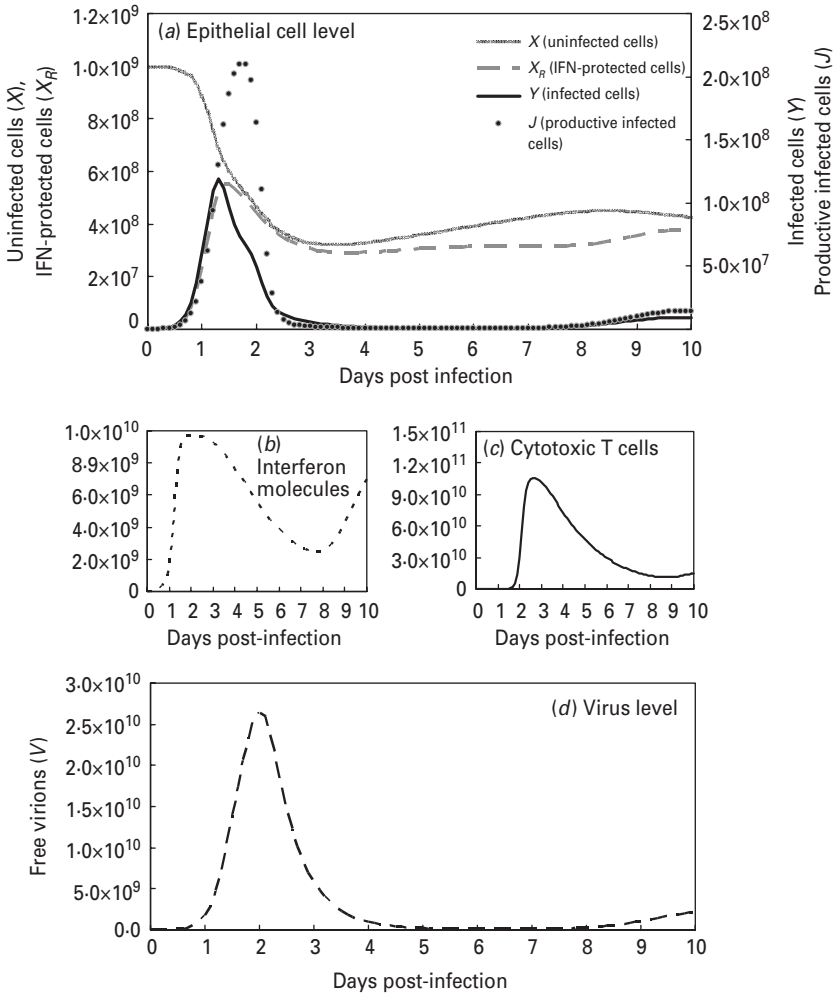

Fig. 5. Model influenza A variables with optimal Pearson correlation analysis ($\beta = 5 \times 10^{-10}$; Table 4) at: (*a*) the epithelial cell level with parameters X (uninfected cells), X_R (IFN-protected cells), Y (infected cells), and J (productive infected cells); (*b*) the human immune response level with parameters I (interferon molecules); (*c*) [Z (CTLs)] and (*d*) the virus level with the parameter V (free virons).

the three additional parameters of IFN-protected cells (X_R), CTLs (Z), and IFN molecules (i). Overall, this inclusion improved experimental data fitting. Therefore, the modified model we developed described appropriately the available experimental data.

The complexity of the model is determined by the purpose of the study and the amount of information in the dataset. As a rule of thumb, it is not advantageous to use a more complex model when a simpler model provides an adequate fit to the data. Undoubtedly, many factors influence the relationship between primary influenza infection and immune response outcome. Thus, several limitations and difficulties existed in this study. The concentration units used for model validation were different between the experimental free virions shedding data and that of simulated free virions. Handel *et al*. [28] provided the unit conversion for 1 $TCID_{50}$ ml^{-1} of nasal wash as corresponding to nearly 10^2–10^5 free virions at the site of infection. In fact, we think that this is a relatively large range for this conversion. Our goal, however, was not to obtain precise conversion numbers, but to examine the qualitative effects of variation in the infection rate of unprotected epithelial cells and viral production from infected epithelial cells, and how these parameters affect viral dynamics. Besides, no available data so far allowed for validating this conversion.

Furthermore, there is difference in the time-scales in human infection experiments. Many previous studies have focused on the beginning of inoculation and drug administration in that the trials were conducted twice daily [15]. However, several studies were conducted daily with a mean viral titre [29] based on

inoculation on day 0. Hence, we defined the inoculation as the first day (day 0) and estimated the following average viral titres on days 0–8.

When humans are infected by influenza virus, innate immune responses are particularly important as the first line of defence against infection; however, adaptive immune responses are also critical for the ultimate control and clearance of influenza A virus infection [30]. In order to consider the compartmentalization of influenza infection, Hancioglu *et al*. [11] and Lee *et al*. [31] proposed more complex models to simulate human immune response to influenza A virus infection in different situations with different objectives. The major difference between our study and the above two studies rests in the number of immune response parameters used for modelling. In the present study, we constructed a simple model of viral dynamics by using three parameters based in part on models developed previously, whereas Hancioglu *et al*. [11] and Lee *et al*. [31] used at least twice as many immune response parameters than our model.

In conclusion, by simulating an advanced model of viral dynamics and applying it to experimental infection data of human influenza, we obtained important estimates of the infection rate of an epithelial cell. This work provides epidemiologically meaningful results and merits further efforts to understand the causes and consequences of influenza pandemics by placing experimental infection data in a predictive framework of viral dynamics in order to develop pertinent mitigation strategies. Our results suggest that the infection rate of an unprotected epithelial cell has an important role in viral dynamics. This modified model could be used for predicting the adaptive immune response [31], antiviral use, or antiviral drug resistance induced by drug selection pressure [32]. Furthermore, it is anticipated that this work could provide an important analytical tool to estimate key parameters in experimental and epidemiological studies related to drug-resistant influenza virus in immune response dynamics. Detailed understanding of system dynamics and interaction between various factors will require further development of the existing analytical models.

ACKNOWLEDGEMENTS

This study was financially supported by National Science Council of Taiwan, Republic of China under Grant NSC 97-2314-B-040-006-MY2.

DECLARATION OF INTEREST

None.

REFERENCES

1. **Nowak MA, May RM.** *Virus Dynamics: Mathematical Principles of Immunology and Virology*. Oxford, UK: Oxford University Press, 2000.
2. **Perelson AS.** Modelling viral and immune system dynamics. *Nature Reviews Immunology* 2002; **2**: 28–36.
3. **Van Kerkhove MD, *et al.*** Studies needed to address public health challenges of the 2009 H1N1 influenza pandemic: Insights from modeling. *PLoS Medicine* 2010; **7**: e1000275.
4. **Perelson AS, *et al.*** HIV-1 dynamics in vivo: virion clearance rate, infected cell life-span, and viral generation time. *Science* 1996; **271**: 1582–1586.
5. **Perelson AS, *et al.*** Decay characteristics of HIV-1-infected compartments during combination therapy. *Nature* 1997; **387**: 188–191.
6. **Nowak MA, Bangham CRM.** Population dynamics of immune responses to persistent viruses. *Science* 1996; **272**: 74–79.
7. **Marchuk GI, *et al.*** Mathematical model of antiviral immune response. I. Data analysis, generalized picture construction and parameters evaluation for hepatitis B. *Journal of Theoretical Biology* 1991; **151**: 1–40.
8. **Nowak MA, *et al.*** Viral dynamics in hepatitis B virus infection. *Proceedings of the National Academy of Sciences USA* 1996; **93**: 4398–4402.
9. **Neumann AU, *et al.*** Hepatitis C viral dynamics in vivo and the antiviral efficacy of interferon-alpha therapy. *Science* 1998; **282**: 103–107.
10. **Baccam P, *et al.*** Kinetics of influenza A virus infection in humans. *Journal of Virology* 2006; **80**: 7590–7599.
11. **Hancioglu B, Swigon D, Clermont G.** A dynamical model of human immune response to influenza A virus infection. *Journal of Theoretical Biology* 2007; **246**: 70–86.
12. **Chang DB, Young CS.** Simple scaling laws for influenza A rise time, duration, and severity. *Journal of Theoretical Biology* 2007; **246**: 621–635.
13. **Chen SC, *et al.*** Viral kinetics and exhaled droplet size affect indoor transmission dynamics of influenza. *Indoor Air* 2009; **19**: 401–413.
14. **Hayden FG, *et al.*** Local and systemic cytokine response during experimental human influenza A virus infection. *Journal of Theoretical Biology* 1998; **101**: 643–649.
15. **Hayden FG, *et al.*** Use of the oral neuraminidase inhibitor oseltamivir in experimental human influenza. *Journal of the American Medical Association* 1999; **282**: 1240–1246.
16. **Hayden FG, *et al.*** Safety and efficacy of the neuraminidase inhibitor GG167 in experimental human influenza. *Journal of the American Medical Association* 1996; **275**: 295–299.

17. **Fritz RS, *et al.*** Nasal cytokine and chemokine responses in experimental influenza A virus infection: results of a placebo-controlled trial of intravenous zanamivir treatment. *Journal of Infectious Diseases* 1999; **180**: 586–593.
18. **Calfee DP, *et al.*** Safety and efficacy of intravenous zanamivir in preventing experimental human influenza A virus infection. *Antimicrobial Agents and Chemotherapy* 1999; **43**: 1616–1620.
19. **Murphy BR, *et al.*** Evaluation of influenza A/Hong Kong/123/77(H1N1) *ts*-1A2 and cold-adapted recombinant viruses in seronegative adult volunteers. *Infection and Immunity* 1980; **29**: 348–355.
20. **Bocharov GA, Romanyukha AA.** Mathematical model of antiviral immune reponse III. Influenza A virus infection. *Journal of Theoretical Biology* 1994; **167**: 323–360.
21. **Beauchemin C, Samuel J, Tuszynski J.** A simple cellular automaton model for influenza A viral infection. *Journal of Theoretical Biology* 2005; **232**: 223–234.
22. **Barroso L, *et al.*** Efficacy and tolerability of the oral neuraminidase inhibitor peramivir in experimental human influenza: randomized, controlled trails for prophylaxis and treatment. *Antiviral Therapy* 2005; **10**: 901–910.
23. **Helton JC, Davis FJ.** Illustration of sampling-based methods for uncertainty and sensitivity analysis. *Risk Analysis* 2002; **22**: 591–622.
24. **Keeling MJ, Rohani P.** *Modeling Infectious Diseases in Humans and Animals*. NJ, USA: Princeton University Press, 2008.
25. **Mogensen SC, Virelizier JL.** The interferon-macrophage alliance. In: Gresser I, ed. *Interferon 8*. London: Academic Press, 1987, pp. 58–84.
26. **Roberts Jr. NJ, *et al.*** Virus-induced interferon production by human macrophages. *Journal of Immunology* 1979; **123**: 365–369.
27. **Murphy BR, Webster RG.** Influenza viruses. In: Fields BN, Knipe DM, Melnick JL, Chanock RM, Roizman B, Shope RE, eds. *Fields Virology*. New York: Raven Press, 1985, pp. 1179–1239.
28. **Handel A, Longini Jr. IM, Antia R.** Neuraminidase inhibitor resistance in influenza: assessing the danger of its generation and spread. *PLoS Computational Biology* 2007; **3**: e240.
29. **Kaiser L, Briones MS, Hayden FG.** Performance of virus isolation and directigen flu A to detect influenza A virus in experimental human infection. *Journal of Clinical Virology* 1999; **14**: 191–197.
30. **McGill J, Heusel JW, Legge KL.** Innate immune control and regulation of influenza virus infections. *Journal of Leukocyte Biology* 2009; **86**: 803–812.
31. **Lee HY, *et al.*** Simulation and prediction of the adaptive immune response to influenza A virus infection. *Journal of Virology* 2009; **83**: 7151–7165.
32. **McCaw JM, *et al.*** Impact of emerging antiral drug resistance on influenza containment and spread: influence of subclinical infection and strategic use of a stockpile containing one or two drugs. *PLoS One* 2008; **3**: e2362.
33. **Treanor JJ, *et al.*** Intranasally administered interferon as prophylaxis against experimentally induced influenza A virus infection in humans. *Journal of Infectious Diseases* 1987; **156**: 379–383.
34. **Hayden FG, *et al.*** Oral LY217896 for prevention of experimental influenza A virus infection and illness in humans. *Antimicrobial Agents and Chemotherapy* 1994; **38**: 1178–1181.
35. **Murphy AW, *et al.*** Respiratory nitric oxide levels in experimental human influenza. *Chest* 1998; **114**: 452–456.